CrossMark

Damping control for a target oscillation mode using battery energy storage

Yongli ZHU[1], Chengxi LIU[1], Bin WANG[1], Kai SUN[1]

MPCE

Abstract In this paper, a battery energy storage system (BESS) based control method is proposed to improve the damping ratio of a target oscillation mode to a desired level by charging or discharging the installed BESS using local measurements. The expected damping improvement by BESS is derived analytically for both a single-machine-infinite-bus system and a multi-machine system. This BESS-based approach is tested on a four-generator, two-area power system. Effects of the power converter limit, response time delay, power system stabilizers and battery state-of-charge on the control performance are also investigated. Simulation results validate the effectiveness of the proposed approach.

Keywords Battery energy storage system (BESS), Battery, Damping ratio, Energy storage, Power system oscillation, State of charge (SOC)

✉ Kai SUN
  kaisun@utk.edu

  Yongli ZHU
  yzhu16@vols.utk.edu

  Chengxi LIU
  cliu48@utk.edu

  Bin WANG
  bwang13@vols.utk.edu

[1] Department of Electrical Engineering and Computer Science, University of Tennessee, Knoxville, TN 37996, USA

1 Introduction

Power system oscillation, whose frequency typically ranges from 0.2 to 2.5 Hz, often occurs in interconnected power grids, and is one of the major concerns in power system operations [1]. The phenomenon of power system oscillation can be caused by many factors such as insufficient system damping, forced oscillation [2], external periodic load perturbation [3], parametric resonance [4] and modal interaction [5], etc. Conventionally, this problem can be partially solved by fine-tuning the parameters of power system stabilizers (PSSs) of the involved generators. However, for an interconnected bulk power system, the offline tuning of PSS parameters of different generators by a coordinated scheme may involve the regulatory entities from different regions that require high-standard cooperation and information sharing. Furthermore, many researchers proposed to use a centralized control system for online tuning PSSs. However, this approach will also introduce the problems of the time delay and communication cost among different interconnected areas. An alternative option for oscillation damping is to use local flexible AC transmission system (FACTS) devices such as static var compensator (SVC), thyristor controlled series capacitor (TCSC), and static synchronous compensator (STATCOM) to provide extra damping support for the system [6–8]. Basically, those are passive elements/sources alleviating oscillations mainly by controlling reactive power or changing the line admittance.

With the fast development of energy storage and power electronics technologies, many utility-scale battery energy storage systems (BESSs) have been deployed in the power system industry and have participated in the power markets. As an active source, the BESS can be used for balancing the power systems to provide the ancillary services.

Springer

In normal conditions of a power system, a BESS is operated in the normal state, i.e. either charging or discharging in a scheduled mode. However, due to their considerable initial investment, its function can be further exploited not only as a system balancing unit, but also to provide extra damping for system oscillations.

Some studies have been reported in recent literatures [9–15]. In [11], the analysis and design of a BESS controller for a two-machine system are discussed and tested, but the analysis for general multi-machine systems is not comprehensively covered. Designing the damping controller based on certain damping-torque relationships and indices is also a focused topic [12]. Those indices can be regarded as a generalization of the damping-torque coefficients in a single machine infinite bus (SMIB) system and can be combined with classic residual methods [13] in designing the PSS. Regarding robust control for damping oscillation by BESS, there are two mainstreams: linear and nonlinear robust control. In [14], the linear matrix inequality (LMI) method is used, which requires the solving of an optimization problem. In [15], the Port-Hamiltonian formulation and the related controller design method are applied on BESS to improve the transient stability.

This paper investigates this problem from an alternative view point, i.e. symbolically solving the equations regarding eigenvalues and then applying the analytical results on the design of the BESS based damping controller. Typically, the inter-area oscillation mode is the main concern for system operators and can be extremely harmful to power system reliability, which is required high priority to be damped. The method proposed here can damp a target mode to an expected damping ratio and, meanwhile, will not worsen other oscillation modes.

The remaining parts of this paper are organized as follows. In Sect. 2, based on the analysis of the power-electronics converter of a BESS, the model is simplified by a proper approximation. In Sect. 3, the linearized state-space model for a power system with a BESS is derived and the eigenvalues are solved. The solution is then used to design the controller to improve the damping ratio of a target mode to an expected value. Section 4 evaluates the effectiveness of the proposed method on both the SMIB system and the two-area system. Conclusions and discussions about the future work are given in Sect. 5.

2 BESS model for system oscillation study

Typically, a BESS includes a storage part comprised of battery cells and a converter interface called a power conditioning system (PCS), as shown in Fig. 1. The PCS is essentially the set of power converters used to maintain the pre-specified voltage and power output. For the BESS, the
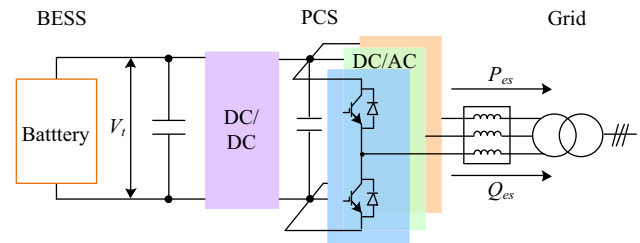

Fig. 1 Topology of grid-connected BESS

PCS is typically composed of a DC/DC converter mainly used for battery charging/discharging control and a DC/AC converter (voltage source converter) mainly used for the AC-grid integration with desired voltage and power output.

Since most grid related control strategies are implemented in the DC/AC stage, in this paper, the PCS is modeled as voltage source converter focusing on the DC/AC part.

2.1 Storage part: battery cells

A battery can be modeled as an equivalent voltage source with the voltage dependent state of charge (SOC). Its equivalent circuit model considering SOC is shown in Fig. 2. Assumptions for this model are: ① the battery can never be discharged to a level under 20%. In this case the voltage is assumed to be linearly dependent on the SOC as shown in Fig. 3 [16]; ② the internal resistance is assumed to be a constant impedance Z, since it is typically very small when the battery is used in high power applications.

With the above assumptions, the equation for the battery is given as:

$$V_t = E_{\max} \cdot SOC + E_{\min}(1 - SOC) - I \cdot Z \tag{1}$$

where $E_{\min}$ is the cell voltage when fully discharged; $E_{\max}$ is the cell voltage when fully charged; Z is the cell internal resistance; I is the cell discharge (> 0)/charge (< 0) current; V_t is the cell terminal voltage.

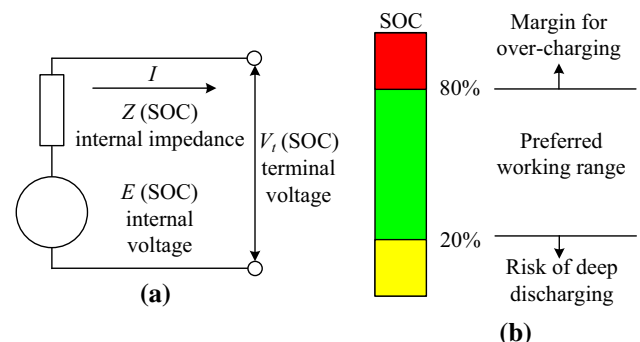In power industry applications, the cell should be protected from deep charging/discharging for life-span

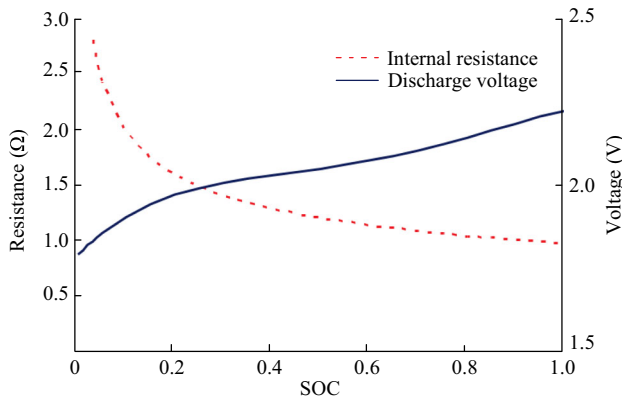**Fig. 2** Equivalent circuit model of battery considering SOC

Fig. 3 Typical discharge profile of lead-acid battery

consideration. An allowable depth of discharge (DOD) is typically 75% or 80% [17]. Thus, a preferable range of SOC is [20%, 80%] in this paper.

2.2 PCS: *P-Q* decoupled control

The classic *P-Q* decoupled control strategy has been widely applied [18, 19]. Figure 4 shows the basic control idea of the outer loop using the signal of frequency or voltage deviation to generate reference values for the inner loop. The inner-loop then generates the pulse width modulation (PWM) signal for the power converter, where P_{ref} and Q_{ref} are the reference values. In this paper, the proposed method focuses on devising the P_{ref}. The inner loop structure as shown in Fig. 5 is the same as the classic *P-Q* decoupled control scheme, which can be found in literature [18, 19]; thus, its details are not expanded here.

2.3 Power output model for BESS

The proposed damping controller adjusts the active power output meanwhile maintaining the BESS reactive output to zero, since the active power and system frequency are highly correlated [20]. Thus, the local generator speed (or approximately the terminal bus frequency) deviation can be used as the input signal for P_{ref}:

$$P_{ref} = -k_{es}\Delta\omega = -k_{es}(\omega - \omega_0) \Leftrightarrow -k_{es}(\omega - 1) \quad (2)$$
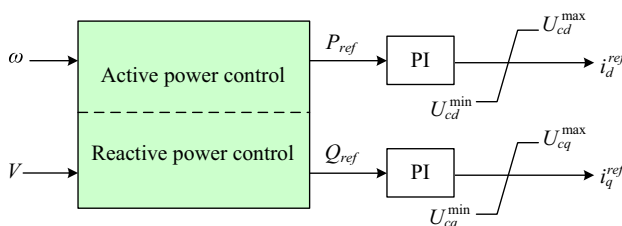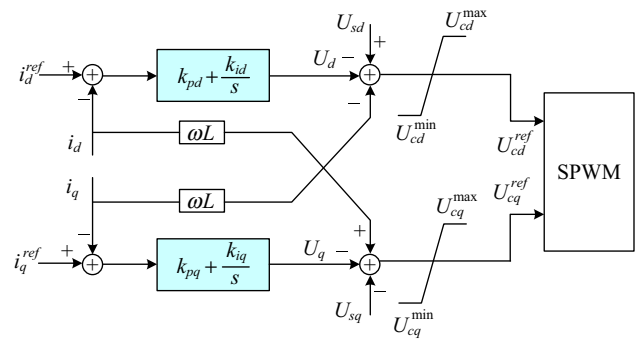

Fig. 5 *P-Q* decoupled control strategy: inner loop

In a typical *P-Q* decoupled control scheme, the active and reactive power can be regulated to their reference values. On the other hand, usually: (1) the response of the power-electronics device (i.e. switching on/off) is much faster than the dynamics of most electromechanical devices, such as synchronous generators; (2) the controller time constants, (e.g. the integral time constants of the PI controller) are typically much smaller than both the cycles of line frequency (e.g. 0.02 s) and the periods of the electromechanical oscillation modes (frequency in the range of 0.2–2.5 Hz). Thus the power output of the BESS can be modeled by a first order transfer function in the power system oscillation study [9, 18] as shown in Fig. 6, where T_{es} is the time constant of the BESS power response.

2.4 Effect of T_{es} on proposed damping control

The effect of T_{es} is slightly reducing the desired damping ratio of the target mode, which will be verified in later sections. T_{es} usually ranges from 0.01 s to 0.05 s, depending on different specifications of the BESS. Thus, in the following section of small signal analysis, T_{es} will be set temporarily to zero during the mathematic derivation, while given as 0.05 s in simulations. Since T_{es} is much smaller than the inertia time constant of a generator [18, 21], in the following analysis, the actual power output of the BESS is approximated by the power output reference, i.e.:

$$P_{es} = \frac{P_{ref}}{1 + T_{es}s} \Rightarrow P_{ref} - P_{es} = T_{es}\frac{dP_{es}}{dt} \approx 0$$
$$\Rightarrow P_{es} \approx P_{ref} = -k_{es}(\omega - 1) \quad (3)$$

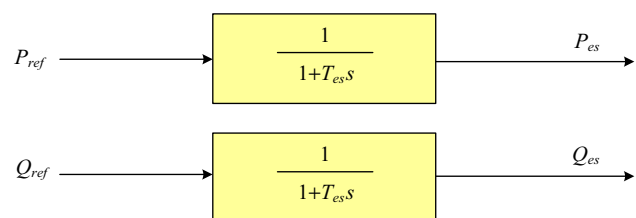Fig. 4 *P-Q* decoupled control strategy: outer loop

Fig. 6 Power output model of BESS used in oscillation study

3 Proposed BESS based damping control

The basic idea of the proposed damping control is:

1) Deriving the analytic relationship between the gain k_{es} in BESS damping controller and the damping ratio ξ for a target oscillation mode.
2) Implementing that gain in the outer-loop controller of the BESS placed nearby the generator's terminal bus.

In the following part, the SMIB system will be investigated first to derive the damping control algorithm. Then, the algorithm will be extended to multi-machine systems having a BESS placed near each generator.

3.1 BESS in SMIB system

3.1.1 Case 1: BESS at generator terminal bus

In Fig. 7, x_1 is the sum of the generator transient reactance x_d' and the transformer reactance x_T, and x is the transmission line reactance.

The system differential algebraic equations (DAEs) are:

$$\begin{cases} \dfrac{\mathrm{d}\delta}{\mathrm{d}t} = \Omega_0(\omega - 1) \\ \dfrac{\mathrm{d}\omega}{\mathrm{d}t} = \dfrac{1}{M}(P_m - P_e - D(\omega - 1)) \\ P_{es} = -k_{es}(\omega - 1) \\ P_{es} + P_e = P_L \approx \dfrac{E_{q0}'V}{x}\sin\delta \end{cases} \tag{4}$$

where $\Omega_0 = 377$ rad/s for 60 Hz system; ω is the generator angular frequency and δ is the rotor angle; E_q' is the transient q-axis voltage of the generator. P_m and P_e are the mechanic power and electric power respectively. P_{es} is the active power output of energy storage. M ($= 2H$) is the generator inertia time constant. The last equation holds approximately in the SMIB system, in which the generator connected to the infinite bus by a long transmission line, i.e. $x_d' + x_T \ll x$.
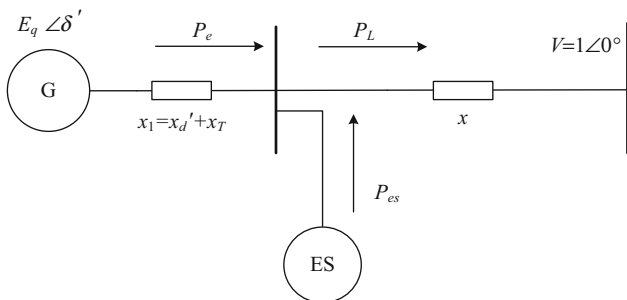

$E_q \angle \delta'$ P_e P_L $V = 1\angle 0°$

G

$x_1 = x_d' + x_T$ x

P_{es}

ES

Fig. 7 Case 1 of SMIB system

Then, linearize (4) around the equilibrium (the quantities with subscript "0" represent the steady-state value, which can be solved from the power flow solution).

$$\begin{cases} \dfrac{\mathrm{d}\Delta\delta}{\mathrm{d}t} = \Omega_0\Delta\omega \\ \dfrac{\mathrm{d}\Delta\omega}{\mathrm{d}t} = \dfrac{1}{M}(\Delta P_m - \Delta P_e - D\Delta\omega) \\ \Delta P_{es} = -k_{es}\Delta\omega \\ \Delta P_{es} + \Delta P_e = \Delta P_L \approx \dfrac{E_{q0}'V}{x}\cos\delta_0\Delta\delta \end{cases} \tag{5}$$

Linearize ΔP_e w.r.t. two state variables $\Delta\delta$ and $\Delta\omega$:

$$\Delta P_e = K_1\Delta\delta + K_2\Delta\omega \tag{6}$$

where K_1 and K_2 are constant coefficients to be determined. Substitute them into the swing equation (5):

$$\dfrac{\mathrm{d}\Delta\omega}{\mathrm{d}t} = \dfrac{1}{M}(\Delta P_m - K_1\Delta\delta - K_2\Delta\omega - D\Delta\omega) \tag{7}$$

Apply Laplace transformation to the swing equation and assume the mechanical power input of generator does not change, i.e. $\Delta P_m = 0$ [21]:

$$\begin{cases} s\Delta\delta(s) = \Omega_0\Delta\omega(s) \\ s\Delta\omega(s) = \dfrac{1}{M}(-K_1\Delta\delta - K_2\Delta\omega - D\Delta\omega) \end{cases} \tag{8}$$

Then, the characteristic equation is:

$$s^2 + \Omega_0\dfrac{(D + K_2)}{M}s + \Omega_0\dfrac{K_1}{M} = 0 \tag{9}$$

Compare it with the standard characteristic equation of a second-order system,

$$s^2 + 2\xi\omega_n s + \omega_n^2 = 0 \tag{10}$$

Equating (9) and (10) yields:

$$\begin{cases} \omega_n = \sqrt{\dfrac{\Omega_0 K_1}{M}} \\ \xi = \dfrac{D + K_2}{2M\omega_n} \end{cases} \tag{11}$$

Then, consider $M = 2H$ in the above expression, we have:

$$\xi = \dfrac{D + K_2}{4H\omega_n} \tag{12}$$

In practice, D needs to be estimated from real system data [23]. For simulation studies, it can be treated as zero if generation and load are modeled in detail [20, 21]. Consider $D = 0$ here, then:

$$K_2 = 4H\omega_n\xi = 8\pi f_n H\xi \tag{13}$$

Therefore, the damping ratio ξ is related to K_2, i.e. the partial derivative of P_e to ω. From the last equation in (5), it then leads to:

$$\Delta P_e \approx \frac{E'_{q0}V}{x}\cos\delta_0\Delta\delta - \Delta P_{es} \approx \frac{E'_{q0}V}{x}\cos\delta_0\Delta\delta + k_{es}\Delta\omega \tag{14}$$

Thus, by (13) and (14) the relationship between ξ and k_{es} is:

$$k_{es} = K_2 = 8\pi f_n H\xi \tag{15}$$

3.1.2 Case 2: BESS at general locations

Now consider a more general case. As shown in Fig. 8, $x_1 = x'_d + x_T + x_{line\text{-}1}$, $x_2 = x_{line\text{-}2}$, where $x_{line\text{-}1} + x_{line\text{-}2} = x$ (i.e. the total reactance of the previous transmission line).

The following (16) and (17) can be derived based on the power balance equation.

$$P_e = \frac{E'_q V_{es}\sin(\delta - \theta)}{x_1} = \frac{V_{es}V}{x_2}\sin\theta - P_{es} \tag{16}$$

$$(E'_q V_{es}\cos(\delta - \theta) - V_{es}^2)x_2 = x_1(V_{es}^2 - V_{es}V\cos\theta) \tag{17}$$

By linearizing (16) and (17), the following expression is finally obtained after some manipulation:

$$\Delta P_e = K_7\Delta\delta + K_8\Delta P_{es} = K_7\Delta\delta - K_8 k_{es}\Delta\omega \atop (\because \Delta P_{es} = -k_{es}\Delta\omega) \tag{18}$$

$$K_8 = \frac{-E'_q(E'_q x_2^2 - 2V_{es0}x_2^2\cos(\delta_0 - \theta_0))}{E'^2_q x_2^2 - 2E'_q V_{es0}x_2^2\cos(\delta_0 - \theta_0)}$$
$$= -\frac{E'^2_q x_2^2 - 2E'_q V_{es0}x_2^2\cos(\delta_0 - \theta_0)}{E'^2_q x_2^2 - 2E'_q V_{es0}x_2^2\cos(\delta_0 - \theta_0)} = -1 \tag{20}$$

$$\Delta P_e = K_7\Delta\delta - \Delta P_{es} = K_7\Delta\delta + k_{es}\Delta\omega \tag{21}$$

It can be noticed that in (21), the coefficient of $\Delta\omega$ is exactly the same as that in Case 1 when neglecting x_1. Finally, k_{es} is given by:

$$\xi = \frac{K_2}{4H\omega_n} = \frac{-K_8 k_{es}}{4H\omega_n} \Rightarrow k_{es} = \frac{8\pi f_n H\xi}{-K_8} \tag{22}$$

To investigate the impact of the BESS installing location, denote $k = x_1/(x_1 + x_2)$. δ is the rotor angle of the generator, typically within $[-\pi/2, \pi/2]$ [20, 21]; E'_q, is the generator transient q-axis voltage with a typical range [0.5, 2.5].

Figure 9 depicts how $-K_8$ changes w.r.t. k for different combinations of δ and E'_q. $-K_8$ achieves its maximum value 1.0 at $x_1 = 0$. When the specified damping ratio ξ is given, the larger $-K_8$ leads to smaller k_{es}. Since k_{es} represents the BESS energy injection/absorption per unit time, a smaller k_{es} means a smaller BESS discharge/charge depth. This will be more attractive for utility companies

$$K_8 = \frac{-E'_q x_2(E'_q x_2 + Vx_1\cos\delta_0 - 2V_{es0}(x_1 + x_2)\cos(\delta_0 - \theta_0))}{E'^2_q x_2^2 + V^2 x_1^2 - 2E'_q V_{es0}x_2^2\cos(\delta_0 - \theta_0) + 2E'_q Vx_2 x_1\cos\delta_0 - 2V_{es0}V(x_1 + x_2)x_1\cos\theta_0} \tag{19}$$

The coefficient K_8 can be named as the "location effect constant" and its expression is given in (19). Then, to check the correctness of this formula for Case 1, letting $x_1 = 0$ and K_8 becomes -1 as shown in (20) and (21).
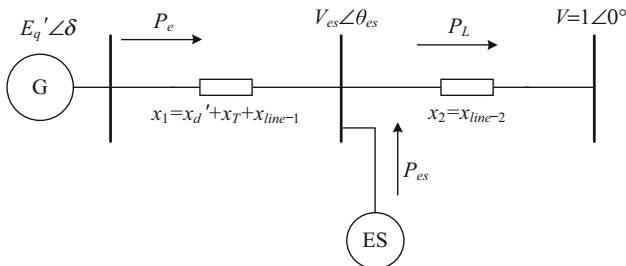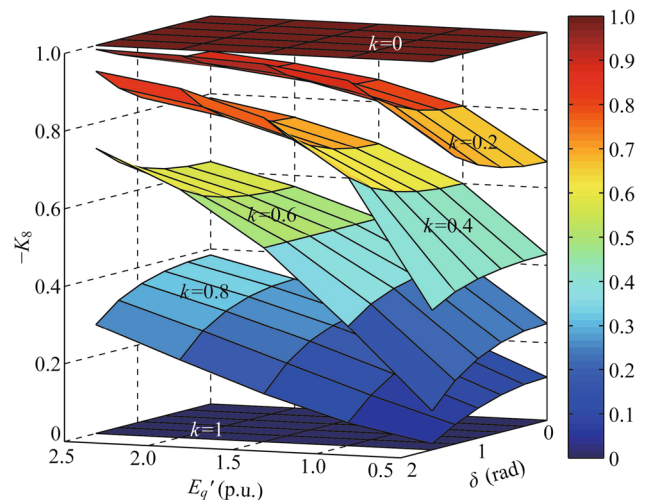

Fig. 8 SMIB system with BESS in Case 2

Fig. 9 Plot of $-K_8$ versus different δ and E'_q under different line ratio k

and system planners, i.e. the BESS can be used as an ancillary service for oscillation damping with potentially lower energy cost.

3.2 BESS in multi-machine system

3.2.1 Small signal state space model

In an n-generator system, similar to the SMIB case, the BESS device can be installed at the terminal buses or nearby buses of generators. As shown in Fig. 10. P_{ei}, P_{esi}, P_{gi} are the electromagnetic power, the BESS output power and active power output of the ith generator respectively.

Apply the reduced network technique [20] by keeping only the generator buses, the system model is:

$$\begin{cases} \dfrac{\mathrm{d}\boldsymbol{\delta}}{\mathrm{d}t} = \boldsymbol{\Omega}(\boldsymbol{\omega} - 1) \\ \dfrac{\mathrm{d}\boldsymbol{\omega}}{\mathrm{d}t} = \boldsymbol{M}^{-1}(\boldsymbol{P}_m - \boldsymbol{P}_e - \boldsymbol{D}(\boldsymbol{\omega} - 1)) \end{cases} \tag{23}$$

$$\boldsymbol{P}_e = \boldsymbol{P}_g - \boldsymbol{P}_{es}$$

where $\boldsymbol{M}^{-1} = \mathrm{diag}[M_i^{-1}]_{n\times n}$; $\boldsymbol{\Omega} = \mathrm{diag}[\Omega_0]_{n\times n}$; $\boldsymbol{\delta} = [\delta_i]_{n\times 1}$; $\boldsymbol{\omega} = [\omega_i]_{n\times 1}$; $\boldsymbol{P}_e = [P_{ei}]_{n\times 1}$; $\boldsymbol{P}_m = [P_{mi}]_{n\times 1}$; $\boldsymbol{P}_{es} = [P_{esi}]_{n\times 1}$; $\boldsymbol{P}_g = [P_{gi}]_{n\times 1}$; $\boldsymbol{D} = \mathrm{diag}(D_1, D_2, \cdots, D_n)$; D_i is the damping constant for the ith generator; P_{gi} can be approximately expressed by [20]:

$$P_{gi} = E_i^2 G_{ii} + E_i \sum_{j=1,\neq i}^{n} E_j(G_{ij}\cos\delta_{ij} + B_{ij}\sin\delta_{ij}) \tag{24}$$

where G_{ij} and B_{ij} are the real and imaginary part of the Y_{ij} in the reduced nodal admittance matrix [21].

Power output of each BESS in a compact form are:

$$P_{esi} = -k_{esi}\Delta\omega_i \Rightarrow \boldsymbol{P}_{es} = -\boldsymbol{K}_{es}\Delta\omega \tag{25}$$

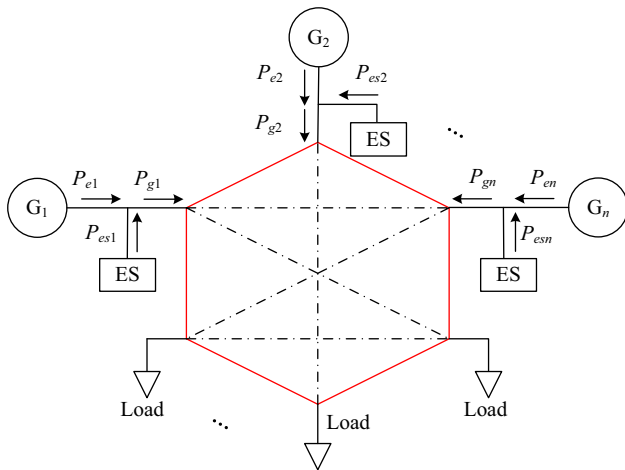where $\boldsymbol{K}_{es} = \mathrm{diag}[k_{esi}]_{n\times n}$, $k_{esi} \geq 0$.

Fig. 10 Multi-machine system with BESS integration

Then, linearize the above equations around the equilibrium point:

$$\begin{pmatrix} \Delta\dot{\boldsymbol{\delta}} \\ \Delta\dot{\boldsymbol{\omega}} \end{pmatrix} = \begin{pmatrix} \boldsymbol{O} & \boldsymbol{\Omega} \\ -\boldsymbol{M}^{-1}\boldsymbol{J}_P(\boldsymbol{\delta}) & -\boldsymbol{M}^{-1}(\boldsymbol{D}+\boldsymbol{K}_{es}) \end{pmatrix} \begin{pmatrix} \Delta\boldsymbol{\delta} \\ \Delta\boldsymbol{\omega} \end{pmatrix} \tag{26}$$

Here, the Jacobian matrix $\boldsymbol{J}_p$ is:

$$\begin{aligned} \boldsymbol{J}_P(\boldsymbol{\delta}) &= \left.\frac{\partial(P_{e1}, P_{e2}, \ldots, P_{en})}{\partial(\delta_1, \delta_2, \ldots, \delta_n)}\right|_{\delta_i = \delta_{i0}} \\ &= \begin{pmatrix} \dfrac{\partial P_{e1}}{\partial\delta_1} & \cdots & \dfrac{\partial P_{e1}}{\partial\delta_n} \\ \vdots & \ddots & \vdots \\ \dfrac{\partial \dot{P}_{en}}{\partial\delta_1} & \cdots & \dfrac{\partial \dot{P}_{en}}{\partial\delta_n} \end{pmatrix}_{\delta_i = \delta_{i0}} \end{aligned} \tag{27}$$

3.2.2 Analytic eigenvalue solutions

Step 1: Determinant simplification

From above section, the $2n$-by-$2n$ system matrix $\boldsymbol{A}$ is:

$$\boldsymbol{A} = \begin{pmatrix} \boldsymbol{O} & \boldsymbol{\Omega} \\ -\boldsymbol{M}^{-1}\boldsymbol{J}_P & -\boldsymbol{M}^{-1}(\boldsymbol{D}+\boldsymbol{K}_{es}) \end{pmatrix} \tag{28}$$

The eigenvalues λ are the roots of the determinant equation:

$$\det(\lambda\boldsymbol{I} - \boldsymbol{A}) = \det\begin{pmatrix} \lambda\boldsymbol{I} & -\Omega_0\boldsymbol{I} \\ \boldsymbol{M}^{-1}\boldsymbol{J}_P & \lambda\boldsymbol{I} + \boldsymbol{M}^{-1}(\boldsymbol{D}+\boldsymbol{K}_{es}) \end{pmatrix} = 0 \tag{29}$$

where $\boldsymbol{I}$ is the identity matrix of n-by-n.

Then the following block matrix lemma is utilized to derive the analytic solution. Its proof can be found in [24].

For matrix $\boldsymbol{M} = \begin{pmatrix} \boldsymbol{A} & \boldsymbol{B} \\ \boldsymbol{C} & \boldsymbol{D} \end{pmatrix}$, if $\boldsymbol{CD} = \boldsymbol{DC}$, then

$$\det\boldsymbol{M} = \det(\boldsymbol{AD} - \boldsymbol{BC})$$

To apply this lemma to (29), it requires:

$$\begin{aligned} &\boldsymbol{M}^{-1}\boldsymbol{J}_P(\lambda\boldsymbol{I} + \boldsymbol{M}^{-1}(\boldsymbol{D}+\boldsymbol{K}_{es})) = (\lambda\boldsymbol{I} + \boldsymbol{M}^{-1}(+\boldsymbol{K}_{es}))\boldsymbol{M}^{-1}\boldsymbol{J}_P \\ &\Rightarrow \boldsymbol{M}^{-1}\boldsymbol{J}_P\boldsymbol{M}^{-1}(\boldsymbol{D}+\boldsymbol{K}_{es}) = \boldsymbol{M}^{-1}(\boldsymbol{D}+\boldsymbol{K}_{es})\boldsymbol{M}^{-1}\boldsymbol{J}_P \end{aligned} \tag{30}$$

Denoting $\boldsymbol{S} = \boldsymbol{M}^{-1}(\boldsymbol{D}+\boldsymbol{K}_{es})$, it is easy to see that $\boldsymbol{S}$ is a diagonal matrix. If $\boldsymbol{S}$ is equal-diagonal, i.e. $\boldsymbol{S} = \mathrm{diag}[S]_{n\times n}$:

$$\frac{(D_1 + k_{es,1})}{M_1} = \frac{(D_2 + k_{es,2})}{M_2} = \cdots = \frac{(D_n + k_{es,n})}{M_n} = S \tag{31}$$

Then, it is easy to verify that (30) can hold.

Thus, if the unknowns k_{esi} are selected based on (31), then (32) can be obtained:

$$\det(\lambda \boldsymbol{I} - \boldsymbol{A}) = \det((\lambda^2 + \lambda \boldsymbol{S})\boldsymbol{I} + \boldsymbol{\Omega}_0 \boldsymbol{M}^{-1} \boldsymbol{J}_P) \quad (32)$$

For matrix product $\boldsymbol{M}^{-1}\boldsymbol{J}_P$, by eigenvalue decomposition [23], it can be transformed to:

$$\begin{cases} \boldsymbol{M}^{-1}\boldsymbol{J}_P = \boldsymbol{T}^{-1}\boldsymbol{\Lambda}\boldsymbol{T} \\ \boldsymbol{\Lambda} = \begin{pmatrix} \mu_1 & \cdots & 0 \\ \vdots & \ddots & \vdots \\ 0 & \cdots & \mu_n \end{pmatrix} \end{cases} \quad (33)$$

where μ_i is the eigenvalue of $\boldsymbol{M}^{-1}\boldsymbol{J}_P$. The real matrix $\boldsymbol{J}_P$ is semi-definite and nearly symmetric [13]. $\boldsymbol{M}^{-1}$ is diagonal. By matrix theory, μ_i is real non-negative number and the above diagonalization process can be guaranteed [24].

Step 2: Analytic solution of each eigenvalue

Apply the Laplace theorem [24] for the determinant of product matrices on (32):

$$\det(\lambda \boldsymbol{I} - \boldsymbol{A}) = \det(\boldsymbol{T}^{-1})\det\big((\lambda^2 + \lambda \boldsymbol{S})\boldsymbol{I} + \boldsymbol{\Omega}_0 \boldsymbol{\Lambda}\big)\det(\boldsymbol{T})$$
$$= \det(\boldsymbol{T}^{-1})\det(\boldsymbol{T})\det\big((\lambda^2 + \lambda \boldsymbol{S})\boldsymbol{I} + \boldsymbol{\Omega}_0 \boldsymbol{\Lambda}\big)$$
$$= \det \underbrace{\big((\lambda^2 + \lambda \boldsymbol{S})\boldsymbol{I} + \boldsymbol{\Omega}_0 \boldsymbol{\Lambda}\big)}_{\text{diagonal}} = \prod_i^n (\lambda^2 + \lambda \boldsymbol{S} + \boldsymbol{\Omega}_0 \mu_i)$$

(34)

Thus, eigenvalues of the original system are the roots for each of the above n quadratic equations, i.e.:

$$\lambda = \frac{-\boldsymbol{S} \pm \sqrt{\boldsymbol{S}^2 - 4\boldsymbol{\Omega}_0 \mu_i}}{2} \quad (35)$$

Furthermore,

If $\boldsymbol{S}^2 - 4\boldsymbol{\Omega}_0 \mu_i \geq 0 \quad \lambda \in R$

If $\boldsymbol{S}^2 - 4\boldsymbol{\Omega}_0 \mu_i < 0 \Rightarrow$ complex roots $(\mu_i > 0)$:

$$\lambda_i = \frac{-\boldsymbol{S} \pm \mathrm{j}\sqrt{4\boldsymbol{\Omega}_0 \mu_i - \boldsymbol{S}^2}}{2} \Leftrightarrow \sigma_i \pm \mathrm{j}\omega_{di}$$
$$= -\xi_i \omega_{ni} \pm \mathrm{j}\sqrt{1 - \xi_i^2}\,\omega_{ni} \Rightarrow$$
$$\begin{cases} \xi_i = \dfrac{\boldsymbol{S}}{2\sqrt{\boldsymbol{\Omega}_0 \mu_i}} \\ \boldsymbol{S} = 2\xi_i \sqrt{\boldsymbol{\Omega}_0 \mu_i} = 2\xi_i \omega_{ni} \\ \omega_{di} = \dfrac{\sqrt{4\boldsymbol{\Omega}_0 \mu_i - \boldsymbol{S}^2}}{2} \end{cases} \quad (36)$$

Step 3: Calculate k_{esi}

To make (31) hold, suppose the kth mode is our target mode (this can be easily identified by its natural oscillation frequency ω_{nk}). Then substitute $\boldsymbol{S} = 2\xi_k \omega_{nk}$ into (31):

$$\frac{D_i + k_{esi}}{M_i} = 2\xi_k \omega_{nk} \Rightarrow k_{esi} = 4H_i \xi_k \omega_{nk} - D_i$$
$$i = 1, 2, \ldots, n \quad (37)$$

Especially when $D_i = 0 \Rightarrow k_{esi} = 4H_i \xi_k \omega_{nk}$.

4 Simulation study

4.1 SMIB system

To test the proposed method for the general location case, the system parameter for the SMIB system are: $x_1 = x'_d + x_{T1} = 0.05 + 0.10 = 0.15$, $x_2 = 0.35$, $k = x_1/(x_1 + x_2) = 0.3$, i.e. about 1/3 of the electric distance between generator and infinity bus. Note that here x_1 is not much smaller than x_2. Mechanical input power $P_m = 1.0$ p.u., $D = 0$ and the nominal frequency $f_0 = 60$ Hz. $K_8 = 0.71898$ by (19).

Two groups of tests on the SMIB system with BESS under different generator inertia parameters ($H = 5$ s and $H = 10$ s) are performed targeting at 5% damping ratio. A three-phase fault is applied at infinite bus from 1 s and cleared at 1.1 s. Prony analysis is used to estimate the actual damping ratio from generator angle and speed waveforms. The results can closely match the expected damping ratio as shown in Table 1. Figure 11 illustrates

Table 1 Control performance of BESS in SMIB Case 2

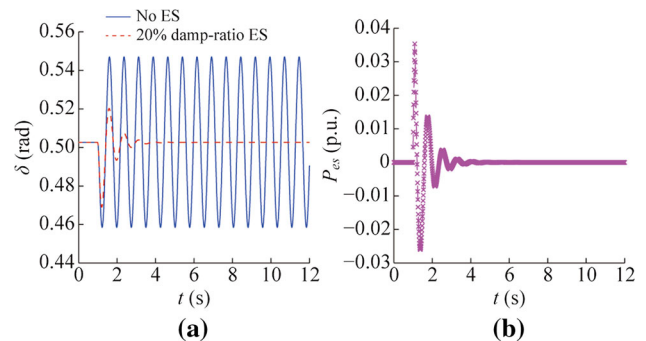| Expected damping ratio (%)	$H = 5$ s		$H = 10$ s	
	Actual damping ratio from Prony analysis (%)	k_{es}	Actual damping ratio from Prony analysis (%)	k_{es}
5	5.009	11.518	5.015	20.036
10	10.03	23.036	10.072	46.072
20	20.16	46.072	20.310	92.144
30	30.37	69.108	30.134	138.22
40	40.21	92.144	40.170	184.29

Fig. 11 Simulation plots for SMIB with 20% damping ratio control

Table 2 Effect of converter time constants T_{es}

Expected damping ratio (%)	T_{es} = 50 ms		T_{es} = 0	
	Actual damping ratio from Prony analysis (%)	k_{es}	Actual damping ratio from Prony analysis (%)	k_{es}
5	4.565	11.518	5.009	11.518
10	9.299	23.036	10.030	23.036
20	19.260	46.072	20.160	46.072
30	30.030	69.108	30.370	69.108
40	40.160	92.144	40.210	92.144
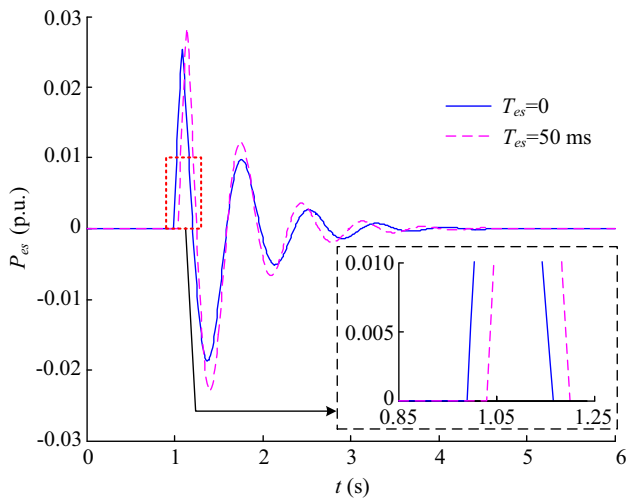
Fig. 12 Comparison of BESS active power response considering T_{es}

the 20% damping ratio case to compare with the original system without BESS. Note that a damping ratio of 5% is usually enough for power system operations; here the test damping ratio ranges from 5% to 40% in order to verify the accuracy of the derived formula by simulations.

If the impact of T_{es}, i.e. the converter time constant, is considered, generally it will slightly reduce the expected damping ratio. In real power converters, T_{es} can be up to

50 ms. Consider the worst case here i.e. T_{es} = 50 ms. The result is listed in Table 2 for the case with $H = 5$ s.

From Table 2, the maximum reduction of damping ratio is only 20.16% − 19.26% = 0.009 for 20% case, so the negative impact of T_{es} is not severe for the proposed control method. A comparison on the active power output of the BESS for $\xi = 20\%$ is shown in Fig. 12.

4.2 Two-area system

In this section, the Kundur's two-area system model [21] is used to investigate the performance of the proposed method on a multi-machine power system. The single line diagram is shown in Fig. 13. The simulation model is built in DIgSILENT/PowerFactory. The battery storage device is modeled by the DIgSILENT simulation language (DSL) [22].

By modal analysis, the system has three oscillation modes: (1) 0.548 Hz with a damping ratio of 4.38%, is an inter-area mode between Area-1 (G1, G2) and Area-2 (G3, G4); (2) 1.002 Hz with a damping ratio of 4.86%; (3) 1.036 Hz with a damping ratio of 4.92%. The last two are local modes. The 0.548 Hz mode has the weakest damping, so its damping ratio needs to be improved. In simulation, a temporary three-phase ground fault is added at bus-8 at 2 sec and cleared after 0.02 s. The objective damping ratio is set to 5%. By (37), the k_{esi} ($i = 1 \sim 4$) is:

$$\begin{cases} k_{esi} = 4H_i\xi_1\sqrt{\Omega_0\mu_1} - D_i \approx 4H_i\omega_{n1}\Delta\xi_1 \\ \Delta\xi_1 = (\xi_1^* - \xi_1) \end{cases} \tag{38}$$

where $\xi_1^* = 5\%$ and ξ_1 is 4.38%, $\omega_{n1} = 2\pi f_{n1}$ is the natural oscillation frequency for mode-1, i.e. the target mode.

4.2.1 Case a: adding BESS in original system

Control effects on three modes are shown in Table 3. It can be observed that the damping ratios of all the three modes have been improved. The improvement for the target mode is the most significant and reaches the 5% goal.
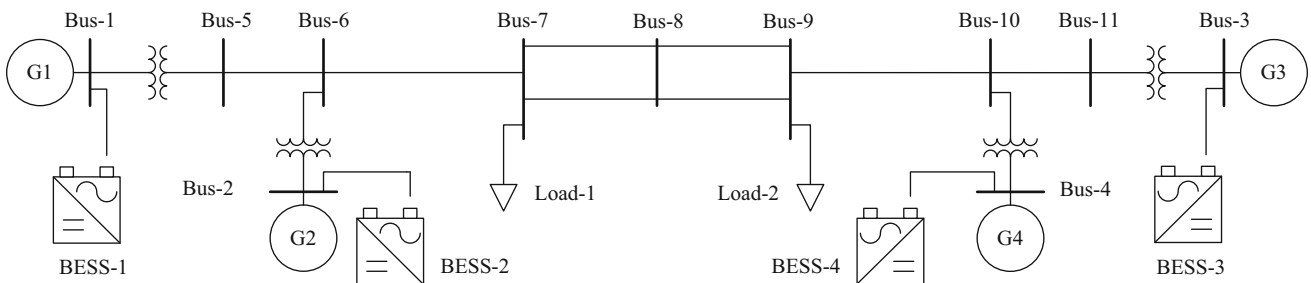

Fig. 13 Single line diagram of the Kundur two area system

Table 3 Control effect of BESS on each mode

Oscillation modes (Hz)	Without BESS		With BESS	
	Damping ratio (%)	Frequency (Hz)	Damping ratio (%)	Frequency (Hz)
0.548	4.38	0.54865	5.04	0.54857
1.002	4.86	1.00218	5.00	1.00205
1.036	4.92	1.03642	5.06	1.03628

In Table 4, the performance of the proposed method is tested for expected damping ratios changing from 5% to 10%. Each result is close to the expectation.

4.2.2 Case b: impact of converter power limit

Either for the sake of protecting the power switch device due to their thermal limits or other technical reasons, a realistic power converter will have a power limit, which may have impact on the control effect of the proposed method. On the other hand, utility-scale power converter output levels have been improved in recent years allowing the maximum power limit to reach 5 MW for single utility scale power converter [17, 25]. If considering aggregating configuration of multi-converters like in a wind farm or battery park [25], this limit can be enhanced to 30 MW [25].

Table 4 Control performance test for target mode with BESS

Expected damping ratio (%)	Actual damping ratio of target mode (%)	Actual frequency of target mode (Hz)
5	5.04	0.549
6	5.99	0.548
7	6.93	0.548
8	7.89	0.548
9	8.84	0.548
10	9.79	0.547

Table 5 Control performance test considering BESS power limit

Expected damping ratio (%)	Actual damping ratio of target mode (%)	Actual frequency of target mode (Hz)
5	4.99	0.548
6	5.92	0.548
7	6.92	0.547
8	7.84	0.547
9	8.79	0.547
10	9.71	0.546

To investigate the power limit impact on the proposed control, similar tests are done with results listed in Table 5.

To visually inspect the nonlinear effect of converter power limit, the following case study is presented with a 10% damping ratio requirement for the target mode. Typically, that means more and faster energy injection/absorption from the BESS than 5% damping ratio requirement.

The power limit is set to 3 MW for each BESS. The BESS power output result is shown in Fig. 14. From the plots, it shows that each BESS is in charging state nearly all the time during this disturbance.

The relative generator rotor angles are shown in Fig. 15. Gen-1 and Gen-4 belong to different areas. Thus, δ_{14} mainly reflects the target mode at 0.548 Hz; the other two modes (1.002 Hz and 1.036 Hz) are mainly caused by oscillations between local generators inside each area, as shown by δ_{12} and δ_{34} respectively. Damping improvement for δ_{14} is the most significant. The damping ratios for other two relative angles are also improved. This phenomenon verifies the control effect and is in consistence with the previous modal analysis result.
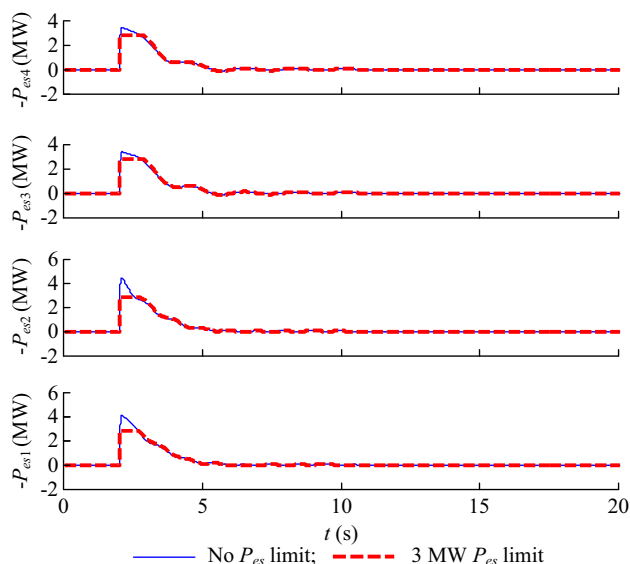

Fig. 14 BESS active power responses for $\xi^* = 10\%$ in Kundur system
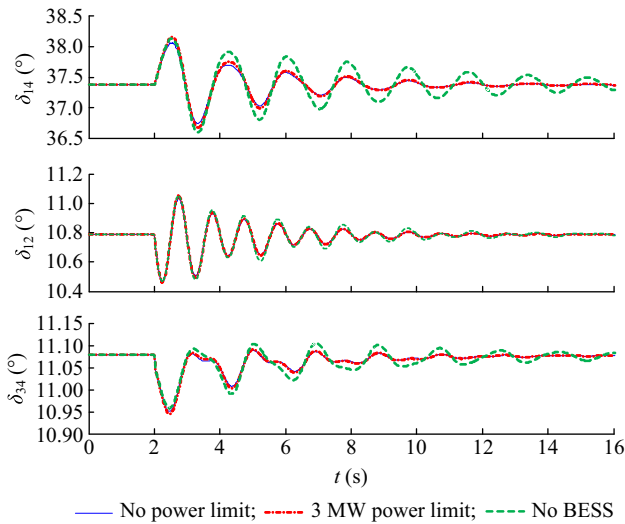
Fig. 15 Relative generator rotor angles for $\xi^* = 10\%$ in Kundur system

4.2.3 Case c: impact of converter time constant T_{es}

Like the previous study in SMIB case, the T_{es} is set to 50 ms. To better demonstrate the impact of T_{es}, no converter power limit is assumed here. Results are shown in Table 6.

In Table 6, as expected, the effect of T_{es} is to slightly lower down the damping ratio, and its largest error is only $9.79\% - 9.688\% \approx 0.001$. This magnitude of error is acceptable in practical power system operations. This result again validates the assumption that, in the proposed method, the converter time constant can be ignored during the analytic formula derivation with small errors introduced. In Table 7, effect on each mode is listed. The target mode can meet the 5% damping ratio goal with other two modes slightly improved as in Table 3.

The BESS power responses are shown in Fig. 16.

4.2.4 Error analysis

The absolute percentage error (APE) of the damping ratio ($|\Delta e| = |\xi - \xi^*|/|\xi^*|$) for the above three cases are compared in Fig. 17, from which there are following

Table 7 Effect of converter time constant T_{es} on each mode

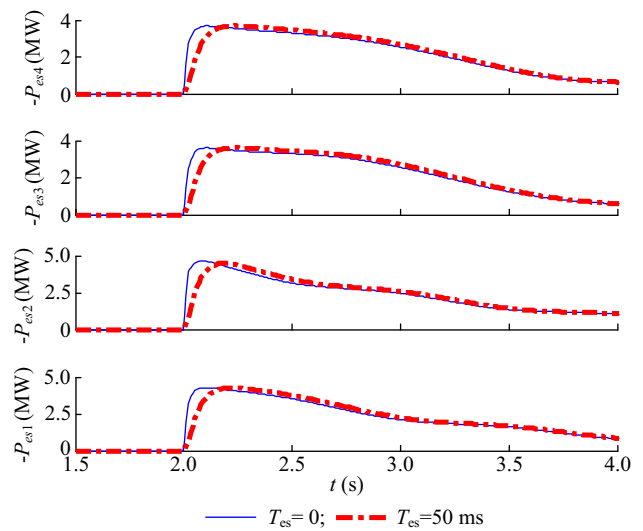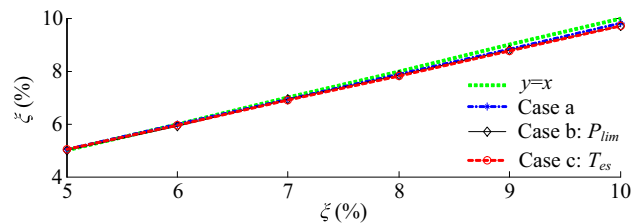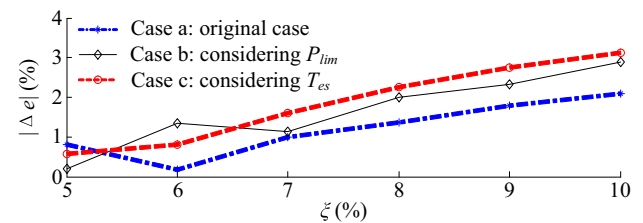| Oscillation modes (Hz)	Before control		After control (T_{es} = 50 ms)	
	Damping ratio (%)	Frequency (Hz)	Damping ratio (%)	Frequency (Hz)
0.548	4.38	0.54865	5.029	0.549
1.002	4.86	1.00218	4.997	1.002
1.036	4.92	1.03642	5.053	1.037

Fig. 16 Zoom-in plot of BESS active power responses when $T_{es} = 50$ ms

(a) Actual damping ratio ξ v.s. expected damping ratio ξ^*

(b) Absolute percentage error $|\Delta e|$

Fig. 17 Performance comparison and error analysis

Table 6 Control performance test considering time constant T_{es}

Expected damping ratio (%)	T_{es} = 50 ms		T_{es} = 0	
	Damping ratio (%)	Frequency (Hz)	Damping ratio (%)	Frequency (Hz)
5	5.029	0.549	5.04	0.549
6	5.951	0.550	5.99	0.548
7	6.888	0.551	6.93	0.548
8	7.819	0.551	7.89	0.548
9	8.753	0.552	8.84	0.548
10	9.688	0.553	9.79	0.547

observations: ① the APE for each case is below 5% which can satisfy practical engineering needs; ② the power converter time constant T_{es} has slightly more influence on the accuracy of the proposed method than other factors, because in the second subplot of Fig. 18, the mean values of APE for the three cases are respectively 1.20%, 1.65% and 1.85%, where the mean APE of case-c considering T_{es} is the largest; ③ the APE will slightly increase with the increase of the desired damping ratio. This can be explained because the proposed BESS controller is essentially a linear type. For most systems, a 5% to 10% damping ratio will be sufficient and reasonable for small-signal stability.

4.2.5 Case study on power system with PSSs

In a real power system, there could be multiple existing PSSs for oscillation damping control. To investigate the damping improvement by the proposed BESS controller on such a system, each generator in the two-area system is equipped with a PSS. All PSSs are designed to make the damping ratio of the target mode reach 4.99% without BESS. Suppose that a higher damping ratio is expected by adding the proposed controller. Then, the new damping ratio goal is set from 6% to 10%, respectively, to design the controller based on (37). The test results are in Table 8. The APE of the damping ratio is depicted in Fig. 18, which are all less than 2%. Note that here ξ_1 in (37) becomes 4.99%, so the calculated value of k_{es} is smaller than its values in previous case studies without a PSS. Since the k_{es}
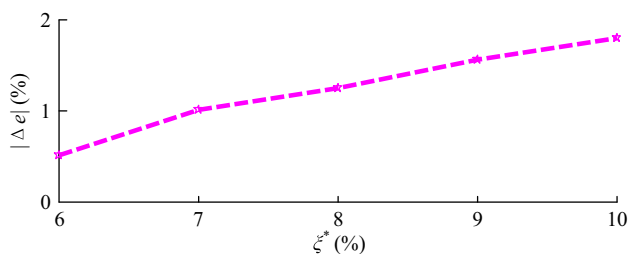

Fig. 18 Error analysis for BESS damping control considering PSS

Table 8 Test results on power system with PSS

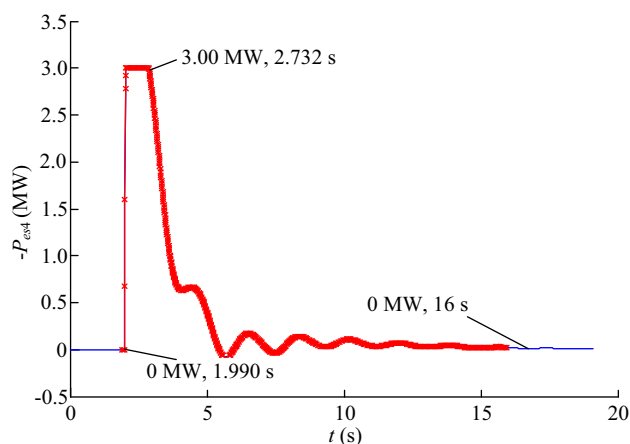| Expected damping ratio (%)	Actual damping ratio of target mode (%)	Actual frequency of target mode (Hz)
6	5.97	0.543
7	6.93	0.542
8	7.90	0.542
9	8.86	0.542
10	9.82	0.542

Fig. 19 Zoom-in plot of BESS-4 active power response

can be interpreted as the power output coefficient of the BESS converter during the disturbance, a smaller k_{es} means a smaller converter capacity required for the BESS. Since the converter capacity takes a major portion of the overall cost of a BESS, the investment on the BESS for damping control in a power system that already has PSSs can be decreased.

4.2.6 Impact on battery SOC

Consider the worst case in subsection-b, i.e. with 3 MW converter power limit for each BESS and 10% damping ratio requirement for the target mode. In Fig. 15, it is observed that the battery is mainly charged during the disturbance. The energy charged is nothing but the area under the power (absorption) curve during disturbance as shown in Fig. 19 (red section) of the zoom-in plot for $-P_{es4}$.

For example, for BESS-4, the energy absorbed is:

$$E_{es4} = \int_{t_0=1.99}^{t=16.0} P_{es4}(t)\mathrm{d}t = 5.6483 \text{ MJ} \Leftrightarrow 0.0016 \text{ MWh}$$

To evaluate the impact on SOC, assume a small energy capacity for BESS-4 (SOCs of other three BESS units can be calculated similarly) as 0.5 MWh (in utility scale BESS, this value can be larger [17, 25]). Then:

Depth of charge = 0.0016/0.5 = 0.0032.

A typical SOC range is [0.2, 0.8]. Thus the theoretical maximum and minimum new SOC are respectively:

$SOC_{new,\max} = 0.8 + 0.0032 = 0.8032$, and the relatively change is only: 0.0032/0.8 = 0.4%;

$SOC_{new,\min} = 0.2 + 0.0032 = 0.2032$, and the relatively change is only: 0.0032/0.2 = 1.6%.

Thus, in both cases the impact on SOC is small, implying that using a BESS for oscillation damping may not weaken its available capacity for other functions like

load following/balancing because the energy provided/absorbed by oscillation is much smaller than the total BESS capacity during disturbance. Moreover, a small portion of energy means potentially a low cost in using BESS for damping oscillation. Due to this fact, the BESS is very promising as a new kind of ancillary service in providing auxiliary damping when needed.

5 Conclusion

This paper proposed a novel damping control method based on the usage of BESS. Analytic eigenvalue solutions were derived on both the SMIB and multi-machine systems. Controller based on those solutions was verified successfully by simulation. The results demonstrated a promising performance in damping target oscillation mode with quantifiable improvement of damping ratio. Thus, to alleviate system oscillations by providing extra damping support based on the proposed method is validated.

Future work includes time delay compensation of the converter time constant for higher control accuracy and studying potential combination of other successful methods like robust control considering parameters uncertainty.

References

[1] Kothari DP, Nagrath IJ (2011) Modern power system analysis. Tata McGraw Hill, New Delhi

[2] Wang B, Sun K (2017) Location methods of oscillation sources in power systems: a survey. J Mod Power Syst Clean Energy 5(2):151–159

[3] Rostamkolai N, Piwko RJ, Matusik AS (1994) Evaluation of the impact of a large cyclic load on the LILCO power system using time simulation and frequency domain techniques. IEEE Trans Power Syst 9(3):1411–1415

[4] Kakimoto N, Nakanishi A, Tomiyama K (2004) Instability of interarea oscillation mode by autoparametric resonance. IEEE Trans Power Syst 19(4):1961–1970

[5] Lin CM, Vittal V, Kliemann W et al (1996) Investigation of modal interaction and its effects on control performance in stressed power systems using normal forms of vector fields. IEEE Trans Power Syst 11(2):781–787

[6] Vahidnia A, Ledwich G, Palmer EW (2016) Transient stability improvement through wide-area controlled SVCs. IEEE Trans Power Syst 31(4):1395–1406

[7] Wang KY, Crow ML (2011) Power system voltage regulation via STATCOM internal nonlinear control. IEEE Trans Power Syst 26(3):1252–1262

[8] Zhang X, Tomsovic K, Dimitrovski A (2016) Optimal investment on series FACTS device considering contingencies. In: Proceedings of the 48th North American power symposium (NAPS), Denver, USA, 18–20 September 2016, 6 pp

[9] Pal BC, Coonick AH, Macdonald DC (2000) Robust damping controller design in power systems with superconducting magnetic energy storage devices. IEEE Trans Power Syst 15(1):320–325

[10] Sui XC, Tang YF, He HB et al (2014) Energy-storage-based low-frequency oscillation damping control using particle swarm optimization and heuristic dynamic programming. IEEE Trans Power Syst 29(5):2539–2548

[11] Beza M, Bongiorno M (2015) An adaptive power oscillation damping controller by STATCOM with energy storage. IEEE Trans Power Syst 30(1):484–493

[12] Shi LJ, Lee KY, Wu F (2016) Robust ESS-based stabilizer design for damping inter-area oscillations in multimachine power systems. IEEE Trans Power Syst 31(2):1395–1406

[13] Pai MA (1989) Energy function analysis for power system stability. Kluwer Academic Publishers, Boston

[14] Fang J, Yao W, Chen Z et al (2014) Design of anti-windup compensator for energy storage-based damping controller to enhance power system stability. IEEE Trans Power Syst 29(3):1175–1185

[15] Kanchanaharuthai A, Chankong V, Loparo KA (2015) Transient stability and voltage regulation in multimachine power systems vis-à-vis STATCOM and battery energy storage. IEEE Trans Power Syst 30(5):2404–2416

[16] Rechargable Batteries Applications Handbook (1992) Technical report, technical marketing staff of Gates Energy Products Inc. Butterworth-Heinemann

[17] Robyns B, François B, Delille G (2015) Energy storage in electric power grids. Wiley, Hoboken

[18] Neely JC, Byrne RH, Elliott RT et al (2013) Damping of interarea oscillations using energy storage. In: Proceedings of IEEE power and energy society general meeting, Vancouver, Canada, 21–25 July 2013, 5 pp

[19] Zhang L (2010) Modeling and control of VSC-HVDC links connected to weak AC systems. Dissertation, KTH Royal Institute of Technology in Stockholm

[20] Anderson PM (2002) Power system control and stability. Wiley-IEEE, Piscataway

[21] Kundur P (1994) Power system stability and control. McGraw Hill, New York

[22] DIgSILENT PowerFactory User Manual (2013) DIgSILENT GmbH, Gomaringen, Germany

[23] Fan L, Wehbe Y (2013) Extended Kalman filtering based real-time dynamic state and parameter estimation using PMU data. Electric Power Syst Res 103:168–177

[24] Horn RA (1990) Matrix analysis. Cambridge University Press, New York

[25] Battery storage power station. https://en.wikipedia.org/wiki/Battery_storage_power_station. Accessed 20 Feb 2017

Yongli ZHU received his B.S. degree and M.S degree from the College of Electrical and Electronics Engineering, Huazhong University of Science and Technology in 2009 and State Grid Electric Power Research Institute in 2012 respectively. He has been working toward the Ph.D. degree at the University of Tennessee in Knoxville since

2014. His research interests include power system stability and control, microgrid modeling and simulation, and machine learning application in power systems.

Chengxi LIU received his B.Eng. and M.Sc. degrees in College of Electrical and Electronic Engineering, Huazhong University of Science and Technology (HUST), China, in 2005 and 2007 respectively. He received the Ph.D. degree at the Department of Energy Technology, Aalborg University, Denmark in 2013. He worked in Energinet.dk, the Danish TSO, until 2016. Currently he is a Research Associate at the Department of EECS, University of Tennessee, USA. His research interests include power system stability and control, renewable energies as well as the applications of artificial intelligence.

Bin WANG received the B.S. and M.S. degrees in electrical engineering from Xi'an Jiaotong University, China, in 2011 and 2013, respectively. He is currently pursuing the Ph.D. degree at the Department of EECS, University of Tennessee in Knoxville. His research interests include power system nonlinear dynamics, stability and control.

Kai SUN received the B.S. degree in automation in 1999 and the Ph.D. degree in control science and engineering in 2004 both from Tsinghua University, Beijing, China. He joined the Department of EECS, University of Tennessee in Knoxville in 2012 and is currently an Associate Professor with that department. He was a Project Manager in grid operations and planning at the EPRI, Palo Alto, CA from 2007 to 2012. His research interests include power system dynamics, stability and control and complex systems. He services in the editorial boards of IEEE Transactions on Smart Grid, IEEE Access, IET Generation, Transmission and Distribution, and Journal of Modern Power Systems and Clean Energy. Dr. Sun received the National Science Foundation CAREER Award in 2016.